

DynaSeg: A Deep Dynamic Fusion Method for Unsupervised Image Segmentation Incorporating Feature Similarity and Spatial Continuity

Boujemaa Guerhazi, Riadh Ksantini, and Naimul Khan, *Senior Member, IEEE*

Abstract—Our work tackles the fundamental challenge of image segmentation in computer vision, which is crucial for diverse applications. While supervised methods demonstrate proficiency, their reliance on extensive pixel-level annotations limits scalability. In response to this challenge, we present an enhanced unsupervised Convolutional Neural Network (CNN)-based algorithm called DynaSeg. Unlike traditional approaches that rely on a fixed weight factor to balance feature similarity and spatial continuity, requiring manual adjustments, our novel, dynamic weighting scheme automates parameter tuning, adapting flexibly to image details. We also introduce the novel concept of a Silhouette Score Phase that addresses the challenge of dynamic clustering during iterations. Additionally, our methodology integrates both CNN-based and pre-trained ResNet feature extraction, offering a comprehensive and adaptable approach. We achieve state-of-the-art results on diverse datasets, with a notable 12.2% and 14.12% mIOU improvement compared to the current benchmarks on COCO-All and COCO-Stuff, respectively. The proposed approach unlocks the potential for unsupervised image segmentation and addresses scalability concerns in real-world scenarios by obviating the need for meticulous parameter tuning.

Index Terms—Unsupervised Learning, Image Segmentation.

I. INTRODUCTION

IN recent years, computer vision has witnessed remarkable strides, driven by the availability of large-scale image datasets as well as the development of advanced machine learning algorithms. Within various real-time applications [1] [2] [3] [4], image segmentation stands out as a pivotal computer vision task, playing a crucial role in interpreting visual content at a granular level. Unlike the straightforward task of image classification, which allocates a category label to the entire image, segmentation involves assigning category labels to individual pixels, effectively outlining the image into meaningful segments or regions. This nuanced approach not only enhances the interpretation of complex scenes, but also contributes to a deeper understanding of visual content.

The segmentation task can be approached from different perspectives, leading to three main types of image segmentation. Semantic segmentation [5] identifies uncountable and

shapeless regions, often referred to as ‘stuff,’ such as grass, sky, or road, based on similar textures or materials. Instance segmentation [6] focuses on pinpointing and segmenting individual instances of countable objects, such as people, animals, and tools, treating them as distinct ‘things.’ Lastly, panoptic segmentation [7] unifies the two distinct concepts used to segment images, assigning a semantic label to each pixel in an image and giving the pixel a unique identifier if it is an object instance. The semantic nuances that differentiate these tasks have led to the creation of methods that employ specialized architectures. Although these task-specific architectures have significantly advanced their segmentation objectives, they need more flexibility to generalize across different segmentation tasks. Variability in the object’s appearance, complex interaction with the object, variations in the object’s scale, and noisy or ambiguous edges complicate the process further.

Classical pioneering segmentation techniques such as active contour models (ACM) [8], k-means [9], and graph-based segmentation (GS) [10] [11] impose global and local data and geometry constraints on the masks. As a result, these techniques are sensitive to initialization and require heuristics such as point resampling, making them unsuitable for modern applications.

The state of the art in segmentation is dominated by deep learning. The Mask R-CNN framework [12] has provided advancement in semantic and instance image segmentation. However, a drawback lies in the substantial requirement for hand-labeled data, limiting the widespread applicability across diverse domains. This challenge becomes particularly pronounced in the context of pixel-wise classification, where the cost of annotation per image is prohibitively expensive.

Unsupervised image segmentation is a possible solution to automatically segment an image into semantically similar regions where the system can find objects, precise boundaries and materials that even the annotation system may not unveil properly. The task has been studied as a clustering problem in the recent literature, with promising results.

Differentiable feature clustering, a state-of-the-art CNN-based algorithm proposed by [13], simultaneously optimizes pixel labels and feature representations through a combination of *feature similarity* and *spatial continuity* constraints [13]. Feature similarity corresponds to the constraint that pixels in the same cluster should be similar to each other. Spatial continuity refers to the constraint that pixels in the same cluster should be next to each other (continuous). However, to achieve the desired segmentation result, [13] applies a manual

Boujemaa Guerhazi is with Electrical, Computer, and Biomedical Engineering, Toronto Metropolitan University, Toronto, Ontario. Email: bguerhazi@ryerson.ca

Riadh Ksantini is with Computer Science, University of Bahrain, Zallaq, Bahrain. Email: rksantini@uob.edu.bh

Naimul Khan is with Electrical, Computer, and Biomedical Engineering, Toronto Metropolitan University, Toronto, Ontario. Email: n77khan@ryerson.ca

Electrical and Computer Engineering, Toronto Metropolitan University, Toronto, ON, Canada e-mail: (see <https://www.torontomu.ca/>).

code will be made available upon manuscript acceptance.

parameter tuning to find the optimal balancing weight μ , which fails to achieve a good balance between the two constraints, as mentioned above, depending on the degree of detail in the image and the dataset.

In this work, we present a novel dynamically weighted loss scheme, offering flexibility in updating the parameters and automatically tuning the balancing weight μ . Our approach conditions the value of μ based on the number of predicted clusters and the iteration number. At each iteration, we dynamically prioritize one of the constraints, resulting in a well-balanced optimization. Key contributions include ¹:

- **Dynamically Weighted Loss:** Introducing a flexible and adaptive loss function that dynamically adjusts the balancing weight μ during training.
- **ResNet with FPN Integration:** Leveraging the power of ResNet with Feature Pyramid Network (FPN) for enhanced feature extraction in the unsupervised segmentation task.
- **Silhouette Score Phase:** Incorporating a silhouette score-based phase to guide the optimization process, ensuring improved cluster quality.

Experimental results across five benchmark datasets demonstrate that our method, DynaSeg, achieves superior quantitative metrics and qualitative segmentation results. The dynamically weighted loss facilitates a more effective balance between feature similarity and spatial continuity, leading to enhanced segmentation performance.

II. RELATED WORK

Machine learning techniques have achieved remarkable success in various vision applications, notably in classification [15] and object detection [16]. Image segmentation in particular has received a lot of research attention.

A. Supervised Segmentation

Recent advances in convolutional neural networks (CNN) and the availability of large annotated datasets have outperformed traditional algorithms [8], [10], which face challenges such as susceptibility to noise, difficulty handling intricate boundaries, and sensitivity to data quality [17]–[19]. Techniques like U-Net [20], SegNet [21], and DeepLab [22] illustrate the effectiveness of CNNs in achieving precise segmentation.

L. Jonathan et al. in [23], inspired by the VGG network [24], introduced FCN, a fully convolutional network with multi-resolution layers for segmentation. Despite these innovations, the FCN result remains blurry, smooth, and unsatisfactory. Afterward, O. Ronneberger in [20] proposed a U-net autoencoder with fewer annotated images and a reasonable training time, addressing the scarcity of training images in biomedical applications.

In [12], Kaiming et al. present Mask R-CNN, an extension of Faster R-CNN [12], incorporating a branch for predicting an object mask alongside the existing branch for bounding box recognition. Following the success of Mask R-CNN, several

deep neural architectures have been proposed recently, such as transformers [25] and capsule networks [26], showing promising results. However, their reliance on hand-labelled data escalates annotation costs and introduces challenges related to missing labels, small datasets, and low resolution [27]–[29].

While supervised segmentation provides excellent results on benchmark datasets, real-life application becomes costly due to its heavy dependence on annotated data. This inherent limitation has resulted in the rise of recent unsupervised segmentation models, including our proposed model, which operates effectively in the absence of explicit annotations, addressing the need for scalable and cost-efficient segmentation solutions.

B. Unsupervised Segmentation

Unsupervised segmentation methods have recently emerged as a cost-effective alternative, aiming to discover objects, boundaries, and materials without explicit ground truth. We divide our discussion into two subsections discussing clustering and CNN-based approaches.

1) *Unsupervised Clustering for Segmentation* : At the forefront of unsupervised segmentation methodologies, Invariant Information Clustering (IIC) [30], and its versions [31] operate at the edge level, training a neural network to form semantic clusters without the need for postprocessing. However, its reliance on enforcing a uniform distribution over clusters makes it particularly effective with well-balanced datasets [28], [29]. Yet, the efficacy of domain knowledge-based approaches, including IIC [30], is contingent upon data balance and can be influenced by the specific data augmentation strategy employed [32]–[34].

To address the challenges associated with IIC and similar techniques, unsupervised segmentation, traditionally framed as a clustering task, leverages methods like K-means [9] and graph-based segmentation (GS) [10]. These approaches utilize features such as color and pixel information to discern meaningful structures within the data. However, K-means struggles with continuous areas due to its inherent sharp boundary assumptions, while GS strikes a balance between preserving details in low-variability regions and ignoring high-variability ones across image regions.

Inspired by the principles of unsupervised segmentation methods, our model adopts a similar clustering strategy. By optimizing clustering loss, we aim to enhance the feature space, accounting for high-level visual similarity. Importantly, our model eliminates the need for a postprocessing phase, streamlining the segmentation process and offering a more efficient and effective solution.

2) *CNN-based Unsupervised Approaches*: Recent advancements in deep learning and convolutional neural architectures enable effective clustering in well-embedded feature spaces. CNN-based unsupervised approaches can be categorized into two groups: discriminative models and generative models.

a) *Generative Models*: Generative Adversarial Networks (GANs) map latent codes to images, generating foreground and background separately. Melas-Kyriazi [35] proposes a GAN-based method for unsupervised foreground-background

¹A preliminary version of this work was published in [14].

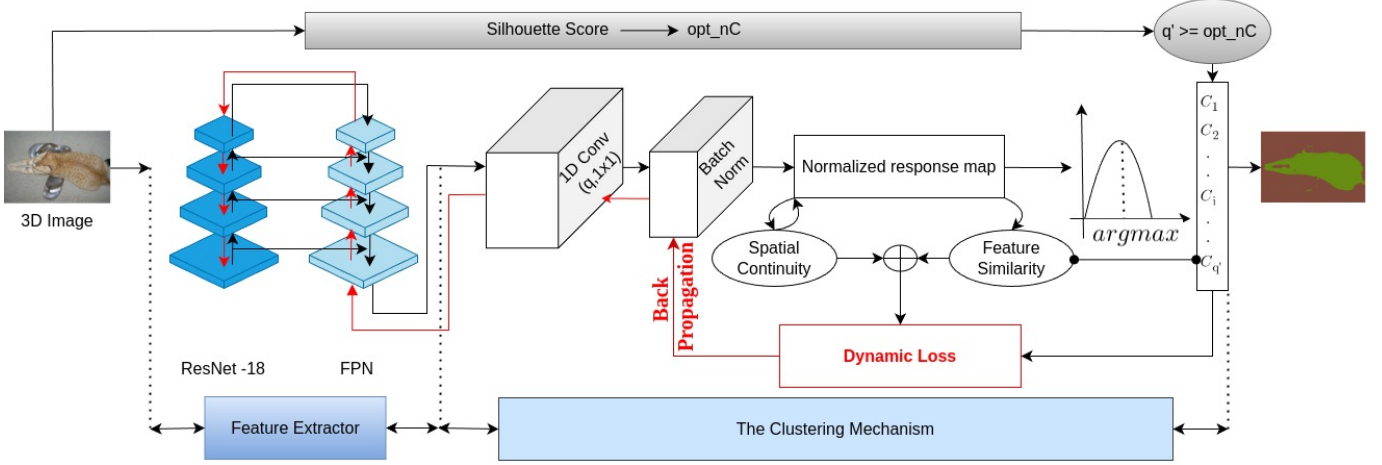


Fig. 1. DynaSeg: Dynamic Weighting Scheme for Unsupervised Image Segmentation Framework. This framework involves a forward-backward process that is iterated T times to obtain the final prediction of the cluster labels c_n .

separation. Leveraging pre-trained GANs like BigBiGAN [36], this approach extracts salient object segmentation from the latent space. However, it relies on class supervision. Labels4Free [37] augments Style-GAN2 [38], introducing a segmentation branch for unsupervised foreground object segmentation. These generative models often focus on binary clustering, distinguishing a specific foreground object.

b) Discriminative Models: In contrast to generative models, discriminative models focus on multi-classification. Wnet [39] exemplifies this approach by combining two U-net [20] structures into an auto-encoder, followed by a postprocessing phase for segmentation refinement. While effective, this method is computationally expensive and requires extensive hyperparameter tuning.

Another discriminative model, Deep Image Clustering (DIC) [40], takes a cost-effective route by breaking down the segmentation problem into two steps: a feature transformation sub-network and a trainable deep clustering sub-network. However, it relies on superpixels, introducing predetermined boundaries.

Infomax [41] presents an alternative where an input image is partitioned into superpixels. The Region-Wise-Embedding (RWE) extracts a feature embedding for each superpixel region, and Mutual-Information-Maximization is employed with adversarial training. Despite its efficiency, challenges persist in recognizing classes due to inherent similarities.

Moving beyond traditional methods, Pixel-wise Clustering Information Extraction (PICIE) [42] introduces a Siamese perspective to unsupervised segmentation, emphasizing equivariance learning. This ensures consistent clustering assignments across different image views and mitigates issues related to hyperparameter sensitivity and dataset imbalance.

Inspired by PICIE, DenseSiam [43] adopts a focus on learning dense representations through contrastive learning and clustering-based techniques, incorporating the class-balanced

cross-entropy loss. However, these methods introduce additional computational operations, potentially struggling with unknown transformations.

In contrast to approaches relying on intermediate representations followed by postprocessing [39]–[41] or being limited to known transformations [42], [43], our alternative strategy, inspired by Kim et al. [13], jointly optimizes pixel labels and features. This process, utilizing the backpropagation of the feature similarity loss and a spatial continuity loss, efficiently generates compact clusters. We emphasize dynamic optimization of the clustering loss to enhance the feature space, addressing challenges posed by superpixels in [44] and the data sensitivity associated with weight coefficients in [13].

III. METHODOLOGY

A. Model Architecture

Our unsupervised image segmentation model, as illustrated in Figure (1), is designed to capture complex patterns and structures within images effectively. Building upon the architecture introduced in our preliminary work [14], we present further enhancements tailored to adapt to varying image content. The architecture comprises three main components: a Feature Extractor Network, a Dynamic Weighting Scheme, and a Clustering Mechanism.

The model, DynaSeg, is shown in Figure (1), where the Feature Extractor Network is employed to produce a p -dimensional feature map r . A final linear classifier layer classifies the features of each pixel into q classes. A batch normalization function is applied to the response map r to obtain a normalized map r' . Lastly, the argmax function is utilized to select the dimension that has the maximum value in r' . Each pixel is assigned the corresponding cluster label c_n , identical to allocating each pixel to the closest point among the q' representative points.

During backward propagation, the loss L (defined in the next section) is calculated. Subsequently, the convolutional filters’ parameters and the classifier’s parameters are updated using stochastic gradient descent. This forward-backward process is iterated T times to obtain the final prediction of the cluster labels c_n . The segmentation problem is handled in an unsupervised manner without knowing the exact number of clusters, making it flexible according to the content of the image. Initially, a large number q is allocated to the initial cluster labels q' . Subsequently, similar or spatially related pixels are iteratively integrated to update the number of clusters q' .

The Feature Extractor Network is the initial processing stage responsible for extracting high-level features from input images. In our extended model, we explore two alternatives for feature extraction: a CNN-based Network comprising M convolutional components and a pre-trained ResNet [45] with a decoder. This exploration allows us to compare and leverage the strengths of each approach for improved image segmentation.

Simultaneously, the Dynamic Weighting Scheme dynamically adjusts the weighting parameter (μ) during iterations, introducing two variants: Feature Similarity Focus (FSF) and Spatial Continuity Focus (SCF). This adaptive scheme enables the model to shift its focus between feature similarity and spatial continuity, reducing sensitivity to parameter tuning and enhancing overall segmentation performance.

The Clustering Mechanism assigns cluster labels to pixels based on the features extracted by the network. The clustering is performed iteratively, with the number of clusters dynamically updated based on feature similarity and spatial continuity. The initial (maximum) number of cluster labels q is set to a large value, and through iterative updates, similar or spatially close pixels are integrated, reducing the number of unique cluster labels q' . To prevent under-segmentation, an intra-axis normalization process is introduced, giving preference to a larger q' .

As a novel addition to our methodology, we introduce the Silhouette Score Phase, calculated only once at the first iteration of the raw image. The optimal number of clusters determined by the silhouette score serves as a threshold, preventing convergence to a single cluster and ensuring meaningful segmentation.

The components of DynaSeg work synergistically: the feature extractor captures complex details, the dynamic weighting scheme adapts the model’s focus during training, and the clustering mechanism assigns meaningful labels to pixels. The integration of these components is crucial for achieving state-of-the-art unsupervised image segmentation.

B. Feature Extractor Network

The Feature Extractor Network, functioning as the primary processing stage, is tasked with extracting high-level features from input images. This pivotal role lays the foundation for subsequent stages by unravelling intricate details and capturing nuanced patterns within the input images. In our extended model, we explore two alternatives for feature extraction:

1) *CNN-based Network*: We employ a CNN-based network that comprises M convolutional components. Each component integrates 2D convolution, *Relu* activation, and batch normalization, collectively forming a robust feature extraction pipeline. The output is a p -dimensional feature map x_n .

2) *Pre-trained ResNet with Feature Pyramid Network (FPN) Decoder*: To expand the spectrum of feature extraction, we introduce an alternative feature extractor network—pre-trained ResNet [45]. This integration responds to the need for richer representations in image segmentation.

To tailor the ResNet architecture for segmentation, we eliminate the Global Average Pooling (GAP) and the Fully Connected Layer (FC) typically used in classification tasks. Furthermore, to restore the original size of the image, we employ a decoder. In contrast to a standard decoder that merely upsamples the extracted feature map, we opt for a Feature Pyramid Network (FPN) decoder. FPN involves lateral connections to fuse features from different resolutions. Implementing FPN on top of the output of the Conv5_x layer outputs a p -dimensional feature map x_n , making the height resolution features semantically strong.

This strategic combination leverages ResNet’s depth and FPN’s multi-scale feature integration, enabling the model to capture details at various granularity levels. We aim to achieve more robust and semantically meaningful image segmentation, focusing on practical descriptions.

This architectural choice facilitates the comparison and utilization of strengths inherent in both the CNN-based network and the pre-trained ResNet with a decoder (FPN). This contribution significantly enhances the overall performance of image segmentation, showcasing the effectiveness of our novel approach.

C. Dynamic Weighting Scheme

In this section, we delve into the details of the proposed Dynamic Weighting Scheme aimed at mitigating the sensitivity issue of the balancing parameter μ in our unsupervised image segmentation model.

1) *Loss Function*: To strike a balance between feature similarity and spatial continuity, two pivotal criteria for distinguishing pixel clusters, our methodology incorporates specific loss functions. The feature similarity loss, denoted as L_{sim} (Equation (1)), plays a crucial role in ensuring that pixels with similar features receive identical labels. This loss quantifies the cross-entropy between the normalized response map r'_n and the corresponding cluster labels c_n . Its minimization facilitates the extraction of precise attributes, contributing significantly to segmentation accuracy.

$$L_{sim}(r'_n, c_n) = - \sum_{i=1}^N \sum_{j=1}^q \delta(j - c_i) \ln r'_{i,j}, \quad (1)$$

where r'_n : normalized response; c_n : cluster labels; $\delta(t)$ is the Kronecker delta function defined as:

$$\delta(t) = \begin{cases} 1 & \text{if } t = 0, \\ 0 & \text{otherwise.} \end{cases}$$

Conversely, the spatial continuity loss L_{con} acts as a high-pass filter, ensuring that spatially continuous pixels receive the same label. Defined by Equation (6), L_{con} as the Manhattan Distance $L1$ Norm of horizontal and vertical differences in the response map r'_n . This mitigates the deficiencies caused by superpixels [44], efficiently removing excess labels due to complex patterns or textures and ensuring spatially continuous pixels share the same label.

$$\Delta h_{i,j} = |r'_n(i,j) - r'_n(i,j+1)| \quad (2)$$

$$\Delta v_{i,j} = |r'_n(i,j) - r'_n(i+1,j)| \quad (3)$$

$$L1_h(r'_n) = \sum_{i=1}^H \sum_{j=1}^{W-1} |\Delta h_{i,j}| \quad (4)$$

$$L1_v(r'_n) = \sum_{i=1}^{H-1} \sum_{j=1}^W |\Delta v_{i,j}| \quad (5)$$

$$L_{con}(r'_n) = L1_h(r'_n) + L1_v(r'_n) \quad (6)$$

Equations (2) and (3) quantify the horizontal ($\Delta h_{i,j}$) and vertical differences ($\Delta v_{i,j}$) between adjacent pixels in the response map r'_n , effectively capturing changes along the horizontal and vertical axes. The subsequent computations, as defined by Equations (4) and (5), aggregate the absolute horizontal differences and vertical differences, giving rise to measures $L1_h(r'_n)$ and $L1_v(r'_n)$. These measures represent the cumulative horizontal and vertical changes in the response map, respectively.

The culmination of these individual components is expressed in Equation (6), where $L_{con}(r'_n)$ represents the total spatial continuity loss. This holistic measure is derived by summing both horizontal and vertical components. In essence, Equation (6) succinctly captures the pixel-wise Manhattan distances along both axes, culminating in the $L1$ Norm. This comprehensive measure effectively encapsulates spatial continuity by considering both horizontal and vertical proximity, contributing collectively to the overarching continuity criterion.

The unsupervised segmentation loss function is represented by Equation (7):

$$L = L_{sim}(\{r'_n, c_n\}) + \mu L_{con}(\{r'_n\}), \quad (7)$$

Here, μ represents the weight for balancing.

While the combination of feature similarity (L_{sim}) and spatial continuity (L_{con}) losses in the unified function L yields reasonably accurate unsupervised segmentation results, the parameter μ plays a crucial role and can lead to varying outcomes. The sensitivity to μ is illustrated in Figure (2), underscoring the challenge of selecting an appropriate value. As can be seen, for $\mu = 50$ and $\mu = 100$, the segmentation is coarse, resulting in sky, buildings, and coastal regions. However, the image is further segmented with $\mu = 1$ and $\mu = 5$, where buildings are further segmented into glass buildings, concrete buildings, and different floors. Although

the authors in [13] argue that the value of μ is proportional to the coarseness of segmentation, We see that the results are not consistent, e.g. the segmentation for $\mu = 50$ appears coarser than $\mu = 100$. This poses a problem in practice. Such high sensitivity to the parameter means that for each dataset, this parameter has to be tuned extensively to obtain a result that is semantically more meaningful.

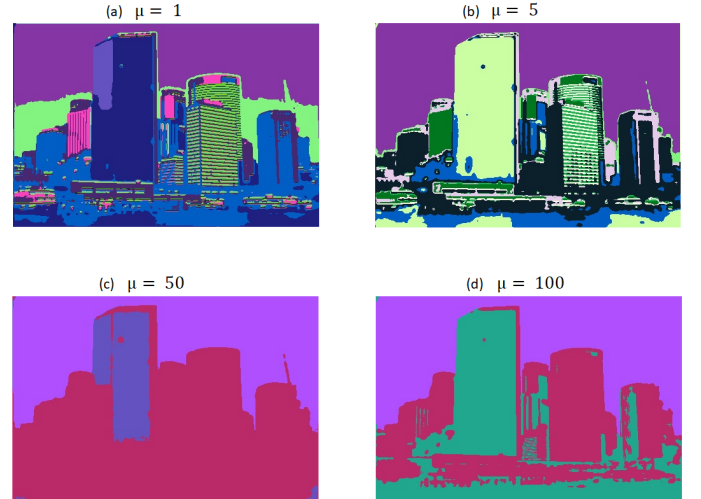


Fig. 2. Results for different μ values on a sample image from the BSD500 dataset.

The competitive nature of both L_{sim} (Feature Similarity Loss) and L_{con} (Spatial Continuity Loss) in our methodology serves to strike a balance between two crucial aspects of unsupervised segmentation:

- **Feature Similarity (Clustering):** L_{sim} encourages pixels with similar features to be grouped into the same cluster. This is vital for capturing the intrinsic similarities among pixels and achieving meaningful clusters representing distinct objects or regions in the image.
- **Spatial Continuity (Smoothness):** Inversely, L_{con} ensures spatially continuous pixels receive the same label. This promotes spatial coherence in the segmentation results and contributes to the smoothness of the segmented regions.

The competitiveness arises from the fact that these two objectives may sometimes conflict. For instance, promoting spatial continuity may result in smoother but less accurate segmentation if not balanced properly with the need to capture fine-grained feature similarities. Conversely, focusing too much on feature similarities may lead to fragmented segmentation without considering the spatial arrangement of pixels. By making L_{sim} and L_{con} competitive, we implicitly guide the model to find an optimal trade-off between capturing feature similarities and maintaining spatial coherence. This competitive interaction helps the unsupervised segmentation model produce results that are both accurate in terms of content and visually coherent.

In our innovative approach to unsupervised image segmentation, we introduce a dynamic weighting scheme that addresses these inherent challenges. Recognizing the significance of adaptability during training, our method incorporates

TABLE I
COMPARISON OF $mIOU$ FOR UNSUPERVISED SEGMENTATION ON BSD500 AND PASCAL VOC2012. BEST SCORES ARE IN BOLD.

Method	dataset				
	<i>BSD500 All</i>	<i>BSD500 Fine</i>	<i>BSD500 Coarse</i>	<i>BSD500 Mean</i>	<i>PASCAL VOC2012</i>
IIC [30]	0.172	0.151	0.207	0.177	0.273
k-means clustering	0.240	0.221	0.265	0.242	0.317
Graph-based Segmentation [10]	0.313	0.295	0.325	0.311	0.365
CNN-based + superpixels [44]	0.226	0.169	0.324	0.240	0.308
CNN-based + weighted loss, $\mu = 5$ [13]	0.305	0.259	0.374	0.313	0.352
DynaSeg - Spatial Continuity Focus (SCF)	0.330	0.290	0.407	0.342	0.396
DynaSeg - Feature Similarity Focus (FSF)	0.349	0.307	0.420	0.359	0.391

a novel dynamic adjustment for the weighting parameter μ . This adjustment responds to the evolving number of predicted clusters and ongoing training iterations, resulting in a flexible and responsive balancing weight.

This dynamic weighting scheme involves changing the weighting parameter’s value during training. We observe that prioritizing feature similarity in the earlier training iterations and gradually shifting focus to spatial continuity (or vice versa) enhances adaptability. The proposed approach introduces a dynamic loss function with a continuous variable μ , where the weight μ dynamically adjusts based on the number of predicted clusters and iterations. We present and compare two versions of this innovative dynamic weighting scheme:

- **Feature Similarity Focus (FSF)**: Initiate the training process by prioritizing the identification of continuous regions, gradually transitioning to a heightened focus on feature similarity. In this case, the performed trials lead to a linear function of the number of clusters (q') for the new dynamic balancing weight $\mu = (q'/\alpha)$ as shown in equation(8). We tried other versions that vary exponentially with the value of q' ; However, such functions resulted in a rapid change in the value of μ , which was not conducive to the balance we sought to achieve between the two constraints.

$$L_{FSF} = L_{sim}(\{r'_n, c_n\}) + (q'/\alpha)L_{con}(\{r'_n\}) \quad (8)$$

- **Spatial Continuity Focus (SCF)**: Initiate training with a focus on feature similarity criteria, gradually transitioning to a stronger emphasis on spatial continuity. In this scenario, the proposed dynamic weight, denoted as μ , takes the form of the multiplicative inverse of the number of clusters, defined as $\mu = (\alpha/q')$ (as shown in Equation (9)). While exploring alternative formulations, including exponential functions, we found that an exponential decay led to an overly rapid change in the value of μ , making it less effective in achieving the desired balance.

$$L_{SCF} = L_{sim}(\{r'_n, c_n\}) + (\alpha/q')L_{con}(\{r'_n\}) \quad (9)$$

2) **Silhouette Score Phase**: We introduce a critical component known as the Silhouette Score Phase to solve an issue in the existing approaches. The clustering model in [13] and [14] only rely on pixel similarity and spatial continuity criteria, assigning the same label to pixels with similar and spatially continuous features. This can lead to a simple solution with $q' = 1$, causing under-segmentation. By evaluating the compactness and separation of clusters, the Silhouette Score acts

as a corrective measure to prevent such under-segmentation issues, ensuring the model achieves a balanced and meaningful segmentation outcome.

The Silhouette Score is a metric widely used in unsupervised learning tasks, particularly clustering, to quantify the goodness of a clustering technique. In the context of our unsupervised image segmentation model, the Silhouette Score Phase operates as follows: at the first iteration of processing the raw image, the Silhouette Score is calculated based on the initial cluster labels. This score serves as a valuable criterion to determine the optimal number of clusters for the given image. By leveraging the Silhouette Score, we introduce a self-regulating mechanism that prevents the model from converging to a single cluster or excessively splitting into numerous small clusters.

D. The Clustering Mechanism

A linear classifier generates a response map $r_n = W_c x_n$, initiating the clustering process. This response map undergoes a normalization step, leading to r'_n with zero mean and unit variance. Employing intra-axis normalization before applying the argmax classification for assigning cluster labels, transforms the original responses r_n into r'_n and introduces a preference for a larger q' , enhancing the model’s adaptability to varying image content. Consequently, the cluster label c_n for each pixel is determined by selecting the dimension with the maximum value in r'_n , a process referred to as the argmax classification. This intuitive classification rule aligns with the overarching goal of clustering feature vectors into q' clusters.

This clustering mechanism assigns each pixel to the closest representative point among the q' points, strategically placed at an infinite distance on the respective axes in the q' -dimensional space. It is noteworthy that C_i can be \emptyset , allowing the number of unique cluster labels to flexibly range from 1 to q' .

In summary, our methodology presents a comprehensive approach to unsupervised image segmentation. The interplay of the Feature Extractor Network, Dynamic Weighting Scheme, and Clustering Mechanism, coupled with the innovative Silhouette Score Phase, contributes to state-of-the-art segmentation performance.

IV. EXPERIMENTAL RESULTS

The objective of our experiments is to showcase the effectiveness of our proposed dynamic weighting scheme for achieving semantically meaningful image segmentation. We

TABLE II
COMPARISON OF DIFFERENT METHODS BASED ON THEIR MEAN INTERSECTION OVER UNION (mIoU) FOR 'STUFF' CATEGORIES AND PIXEL ACCURACY (PACC) ON COCO-STUFF.

Method	Backbone	mIoU Stuff	pAcc
IIC	ResNet18	27.7	21.8
Picie	ResNet18	31.48	50.0
DenseSiam	ResNet18	24.5	...
HSG (Ke et al., 2022)	ResNet50	23.8	57.6
ReCo+ (Shin et al., 2022)	DeiT-B/8	32.6	54.1
DINO (Caron et al., 2021)	ViT-B/8	41.9	74.9
DynaSeg - SCF	CNN-Based	42.41	76.7
DynaSeg - SCF	ResNet-18 FPN	42.41	76.7
DynaSeg - FSF	CNN-Based	42.37	76.6
DynaSeg - FSF	ResNet-18 FPN	54.10	81.1

TABLE III
COMPARISON OF mIOU FOR UNSUPERVISED SEGMENTATION ON COCO-ALL.

Method	Backbone	mIoU All
Modified Deep Clustering	-	9.8
IIC	ResNet18	6.7
Picie	ResNet18	14.4
DenseSiam	ResNet18	16.4
DynaSeg - FSF	CNN-Based	30.51
DynaSeg - SCF	CNN-Based	27.57
DynaSeg - FSF	ResNet-18 + FPN	30.07
DynaSeg - SCF	ResNet-18 + FPN	30.52

conducted extensive evaluations on multiple datasets, comparing against state-of-the-art methods.

A. Experiment Setup

In our experiments, we introduce two versions of the feature extractor: a CNN-based extractor and a pre-trained ResNet-18 [45] with Feature Pyramid Network (FPN). For the CNN-based extractor, we set the number of components in the feature extraction phase, denoted as M , to 3. Conversely, for the ResNet18 with FPN, we modify the output channel to match the number of classes in the dataset (e.g., 27 on COCO stuff-thing dataset).

For consistency across all tests, we set the dimensions of the feature space, p , and the cluster space, q , to be equal, with both values set to 100. We employ a learning rate with a base lr=0.1 and SGD optimizer, where the weight decay is 0.0001, and the SGD momentum optimizer is set to 0.9. The best α for SCF and FSF clustering were experimentally determined from $\{25, 45, \mathbf{50}, 55, 60, 75, 100, 200\}$ and $\{2, 10, \mathbf{15}, 25, 50, 100\}$, respectively. We report results for $\alpha = 15$ for FSF clustering ; $\alpha = 50$ for SCF clustering.

The mean Intersection Over Union ($mIOU$) is reported for the benchmark datasets. It's important to note that ground truth is utilized solely during the assessment phase and plays no role in the training process.

1) *COCO-Stuff*: In accordance with the methodology outlined in [30], [42], [43], we evaluate the performance of our model using the COCO-Stuff dataset [46]. This dataset

is distinguished for its extensive collection of scene-centric images, featuring 80 thing and 91 stuff categories. The model is evaluated on curated subsets [30], [42] of the COCO val2017 split, consisting of 2,175 images. Following the preprocessing procedure detailed in [42], we amalgamate classes to establish 27 categories, comprising 15 stuff and 12 things. It's noteworthy that, unlike earlier studies focusing solely on stuff categories, our evaluation encompasses both things and stuff categories.

2) *BSD500*: Additionally, we utilize the Berkley Segmentation Dataset BSD500 [47] and PASCAL Visual Object Classes 2012 [48] for both quantitative and qualitative evaluation of the segmentation results. The BSD500 dataset comprises 500 color and grayscale natural images. Following the experimental setup in [13], we use the 200 color images from the BSD500 test set to evaluate all models.

3) *PASCAL VOC2012*: For PASCAL VOC2012 [48], we treat each segment as an individual entity, disregarding object classification. The VOC2012 dataset is expansive, containing 17,124 images, of which 2,913 have semantic segmentation annotations. We use the 2,913 semantic segmentation images for evaluating our method. In addition, we utilize select images from the Icoseg [49] and Pixabay [50] datasets to present qualitative results.

B. Evaluation

To assess the performance of the model trained without labels, a correspondence between the model's label space and the ground truth categories must be established. Initially, the model predicts on each image within the validation set. Subsequently, the confusion matrix is computed between the predicted labels and the ground truth classes. Employing linear assignment, we establish a one-to-one mapping between the predicted labels and ground truth classes, with the confusion matrix serving as the assignment cost. The mean Intersection over Union (mIoU) is then calculated over all classes based on this mapping [42], [43]. For a more comprehensive analysis of the model's behavior, we present the mean IoU values for stuff and things classes.

Given the multiple ground truth types in BSD500, we adopt three mIOU counting strategies for assessment: "BSD500 All" considers all ground truth files, "BSD500 Fine" focuses on the ground truth file with the most significant number of segments, and "BSD500 Coarse" considers the ground truth file with the smallest number of segments. We define "BSD500 Mean" as the average of these three measurements.

C. Quantitative Results

The performance of various state-of-the-art methods in unsupervised semantic segmentation is comprehensively evaluated on multiple datasets.

1) *COCO-All Dataset*: Table III presents the results on the COCO-All dataset, comparing mean Intersection over Union (mIoU) scores. The two proposed DynaSeg versions, Feature Similarity Focus (FSF) and Spatial Continuity Focus (SCF), with different backbones, exhibit varying performance. Notably, SCF with ResNet-18 FPN achieves a state-of-the-art

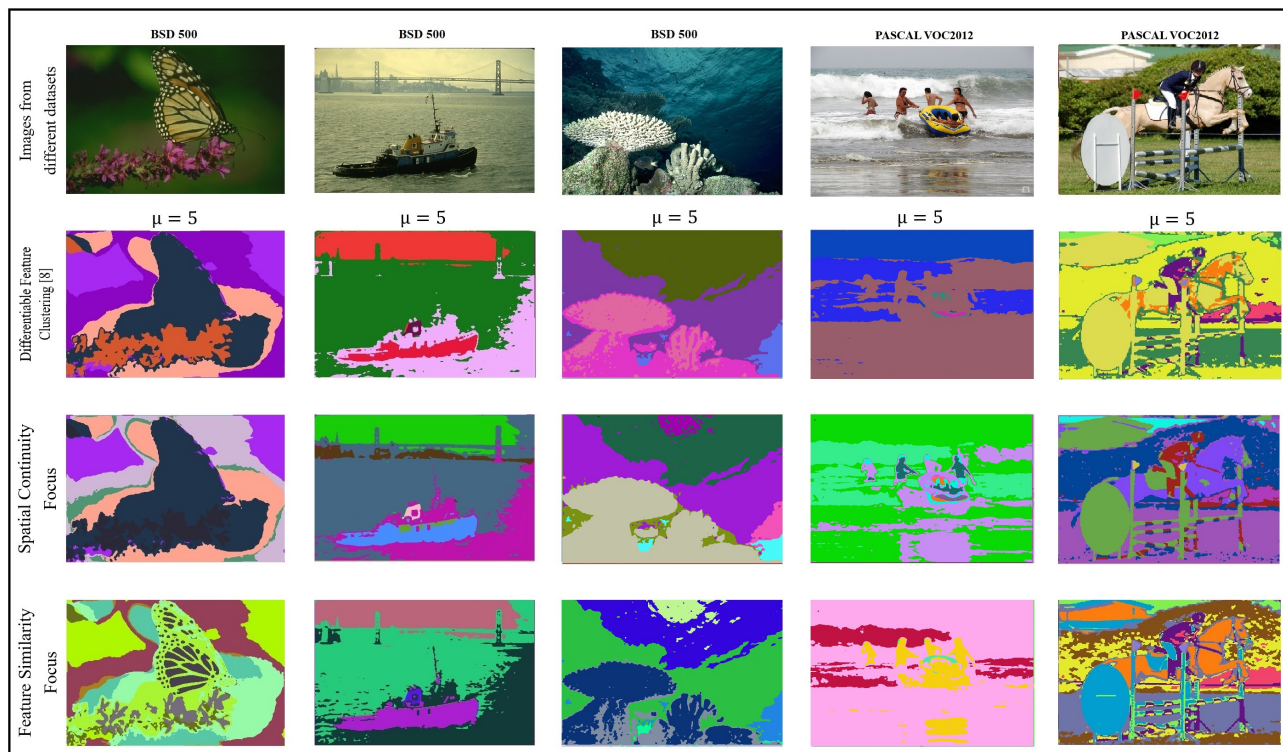


Fig. 3. Qualitative Results on select BSD500 and PASCAL VOC2012 images. Same color corresponds to the pixels being assigned the same clustering label by the algorithm. Please read Section IV-D for discussion on these results.

mIoU of 30.52, surpassing existing benchmarks. SCF outperforms DenseSiam by 14.12 and Picie by 16.08, establishing its leadership in unsupervised semantic segmentation.

2) *COCO-Stuff Dataset*: Table II summarizes the results for the COCO-stuff dataset, considering different backbones and architectures. SCF with CNN-Based achieves an mIoU Stuff of 42.41 and pAcc of 76.7, demonstrating its effectiveness. However, FSF with ResNet-18 FPN emerges as the new state-of-the-art, surpassing all methods with the highest mIoU Stuff of 54.10 and pAcc of 81.1.

3) *BSD500 and PASCAL VOC2012 Datasets*: Quantitative results on BSD500 and PASCAL VOC2012 datasets are detailed in Table I. SCF achieves a remarkable mIOU of 0.396 on PASCAL VOC2012, demonstrating its effectiveness. FSF consistently outperforms other methods on BSD500, emphasizing its robustness across various ground truth types. In addition to quantitative evaluations, we provide a demo [51] of incremental segmentation using DynaSeg on a sample image from the Pascal VOC2012 dataset. This demo is available in the supplemental video, showcasing our method’s application to real-world images.

In summary, the proposed FSF and SCF methods exhibit superior performance across different datasets and evaluation metrics. The achieved results reinforce their effectiveness, establishing them as prominent approaches in unsupervised semantic segmentation.

D. Qualitative Results

We also provide qualitative results on a few images as done in [13]. The qualitative evaluation showcases the segmentation

results for the Spatial Continuity Focus (SCF) method, comparing it with the Differentiable Feature-based Segmentation model (Diff) [13] and the ground truth. In Figure 4, SCF exhibits its strength in accurately capturing complex details of the cat, including fine contours, legs, and tail. The method achieves high-resolution segmentation with nuanced object boundaries, aligning effectively with the ground truth.

Notably, SCF outperforms Diff by providing a clean and accurate representation of the object. Diff, on the other hand, introduces noise in the background and struggles to accurately segment the tail of the cat, often blending it with the background. This emphasizes SCF’s robust performance in preserving true object shapes and minimizing unwanted artifacts, making it particularly effective in complex scenes with detailed structures.

Additionally, As shown in Figure (3), our model is more effective in bringing out segmentation regions that are semantically related. For example, For the “Show Jumping” image (column 5), the horse and the obstacle are classified as the same class by [13] (both yellow). However, for both FSF and SCF, the horse and the obstacle are appropriately distinguished. For the “ship” image (column 2), [13] fails to differentiate between the sky and the body of the ship (both red), but both proposed SCF and FSF can do it successfully.

Further qualitative results are shown for select Icoseg [49] and Pixabay [50] datasets that were also used in [13]. These results can be seen in Figure (5). The qualitative results on these datasets are presented to further demonstrate that our proposed approaches do not require as much parameter tuning as [13] does. Figure (5) highlights that the baseline Differentiable

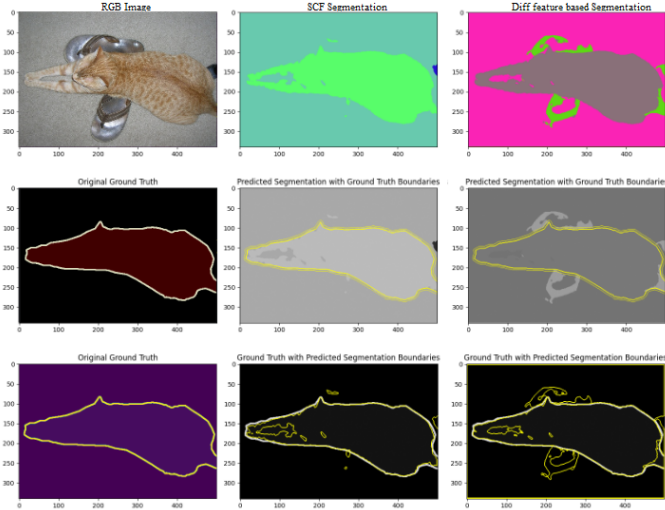


Fig. 4. Qualitative results on Pascal VOC 2012: Original image, DynaSeg - SCF predicted segmentation, and Diff predicted segmentation.

Feature Clustering [13] is quite parameter sensitive. For each dataset, the weighting balance μ must be tuned extensively to obtain a more semantically meaningful result. For instance, PASCAL VOC 2012 and BSD500 datasets require a small balancing value $\mu = 5$. While, Icoseg [49] and Pixabay [50] datasets need a much larger balance value $\mu = 50$ and $\mu = 100$, respectively. On the other hand, As illustrated in Figures (3) and (5), our proposed method has proven effective in dealing with different datasets using the same weight for both FSF and SCF. The proposed methods also bring out details in an unsupervised manner that is semantically more meaningful. For example, using the Feature Similarity Focus method (FSF), the red car from the iCoseg dataset (column 2 row 4 in Figure (5)) displays more detail on the tires and more precise building outlines than the details extracted by [13] (column 2 row 2), where the car is partially blended into the road. Similarly, for the peppers image (column 4 in Figure (5)), [13] was unable to identify the shapes of the individual peppers accurately. Both of our proposed method do a much better job, even with the same value of μ as the other images.

In the comparative analysis of the proposed SCF and FSF methods, SCF exhibits notable proficiency in class segmentation, excelling in delineating distinct categories. Conversely, FSF demonstrates superior performance in instance segmentation tasks. Figure (3) column 3 illustrates this distinction. SCF accurately segments the image into well-defined classes such as water, the surface of the sea, and sea coral. On the other hand, FSF not only identifies these classes but also provides more details, capturing the nuances of sea coral structures, including the main trunk and branches. Notably, in Figure (3) column 1, FSF showcases its capability by revealing fine details of butterfly wing veins and forewing structures with remarkable precision. This precision makes FSF particularly well-suited for applications in the medical domain. The choice between SCF and FSF should be guided by the specific requirements of the given application, considering the emphasis

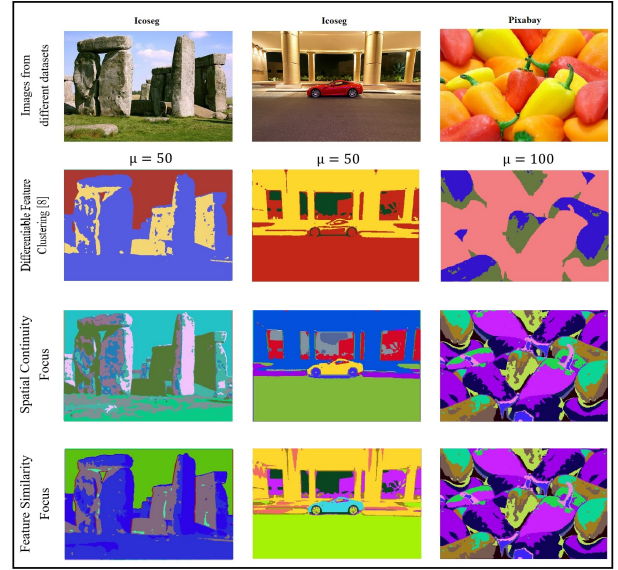


Fig. 5. Qualitative Results on select Icoseg and Pixabay images. Same color corresponds to the pixels being assigned the same clustering label by the algorithm. Please read Section IV-D for discussion on these results.

on either class segmentation or detailed object representation.

The experimental results clearly demonstrate the superiority of our proposed dynamic weighting scheme over existing methods. The SCF and FSF methods consistently outperform other techniques in both quantitative and qualitative assessments. Specifically, the adaptability of the proposed approach to varying datasets and scenarios is evident in the significant improvements achieved in mIoU scores across different datasets and evaluation metrics.

V. ABLATION STUDY

This section presents supplementary results examining the influence of the Silhouette Score Phase and the Feature Extractor through ablation on the COCO dataset. Additionally, we provide a comparison between FSF and SCF to further analyze their respective contributions.

A. Silhouette Score Impact

To evaluate the impact of integrating the Silhouette Score into our proposed dynamic weighting scheme, we conducted an ablation study, comparing segmentation results with and without the inclusion of Silhouette Score. Table IV presents the comparative results across different configurations.

In the case of the FSF method with a CNN-based backbone, integrating Silhouette Score at threshold 3 significantly improves the mIoU for "All" from 26.03 to **30.51** and for "Stuff" from 34.82 to **42.39**, demonstrating substantial enhancements.

For the SCF method with a ResNet-18 backbone, the segmentation results remain consistent for "All," "Things," and "Stuff" across both threshold 3 and Silh.S configurations, indicating that the model itself maintains the number of clusters, which doesn't reach the specified threshold. This implies that the SCF method inherently adjusts its clustering strategy, rendering the additional Silhouette Score less influential in

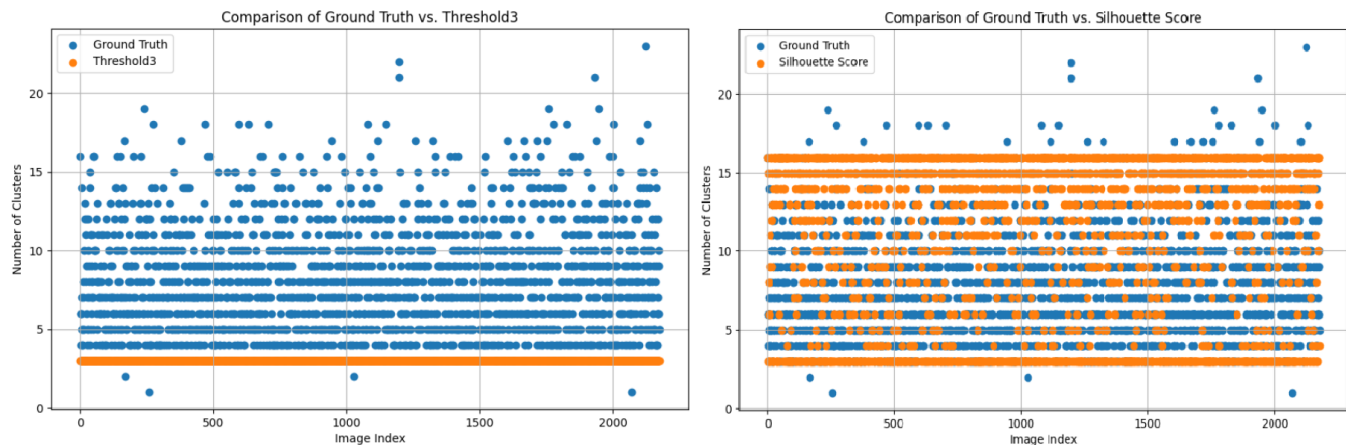


Fig. 6. Comparison of cluster distribution: Left graph shows the comparison of the distribution of the number of clusters in the ground truth (blue) to a fixed threshold of three clusters (orange). Right graph displays the distribution of the number of clusters in the ground truth (blue) and the number of clusters predicted by the silhouette score (orange).

TABLE IV
SILHOUETTE SCORE IMPACT

Framework	Backbone	Threshold	mIoU		
			All	Things	Stuff
DynaSeg - FSF	CNN-Based	3	26.03	61.73	34.82
DynaSeg - FSF	CNN-Based	Silh.S	30.51	74.10	42.39
DynaSeg - SCF	ResNet-18	3	<u>30.52</u>	74.06	42.41
DynaSeg - SCF	ResNet-18	Silh.S	<u>30.52</u>	74.06	42.37

TABLE V
COMPARISON OF FRAMEWORK AND BACKBONE VARIATIONS.

Framework	Backbone	mIoU			pAcc
		All	Things	Stuff	
DynaSeg - FSF	CNN-Based	30.51	74.10	42.39	76.65
DynaSeg - FSF	ResNet-18	30.07	62.87	54.10	81.08
DynaSeg - SCF	CNN-Based	27.57	63.55	35.08	76.34
DynaSeg - SCF	ResNet-18	30.52	74.06	<u>42.37</u>	76.67

this scenario. this nuanced understanding of the SCF behavior underscores the adaptability of the model and its ability to maintain segmentation quality without explicit reliance on external thresholds. It showcases the model’s self-adjusting clustering mechanism, which may result in consistent mIoU values in certain scenarios.

Complementing the tabular results, the accompanying graph provides insights into the distribution of ground truth cluster numbers. On one side, it contrasts the distribution with a random threshold of 3, revealing a substantial disparity. On the other side, the distribution is compared with the optimal number of clusters derived from the Silhouette Score, demonstrating a strong correlation and underscoring the effectiveness of the proposed dynamic weighting scheme.

This combined analysis emphasizes the significance of incorporating the Silhouette Score in our framework, showcasing its positive influence on segmentation accuracy across different scenarios and backbone architectures.

B. Effect of Feature Extractor

To analyze the impact of the choice of feature extractor, we compare the performance of CNN-Based and ResNet-18 with FPN in the FSF and SCF methods. Table V comprehensively compares segmentation results across different combinations of frameworks and backbones.

For the FSF method, the choice of the feature extractor has a substantial impact on segmentation performance. When using a CNN-Based backbone, the mIoU for "All" is 30.52,

and for "Stuff," it is 42.39. In contrast, with a ResNet-18 backbone, the mIoU for "All" decreases slightly to 30.07, but there is a notable improvement in "Stuff" with a mIoU of 54.10. This suggests that the ResNet-18 backbone with FPN captures semantic information related to "Stuff" categories more effectively.

Similarly, for the SCF method, the impact of the feature extractor is evident. With a CNN-Based backbone, the mIoU for "All" is 27.57, and for "Stuff," it is 35.08. Switching to a ResNet-18 backbone results in an improvement, with the mIoU for "All" reaching 30.52 and for "Stuff" reaching 42.37. This highlights that the ResNet-18 backbone, even with its deeper architecture, contributes to better segmentation performance for both the "All" and "Stuff" categories.

The pixel accuracy (pAcc) values further complement these findings, showcasing the overall accuracy of pixel-level predictions. In summary, the choice of feature extractor, particularly the ResNet-18 backbone, plays a crucial role in enhancing segmentation performance, especially for specific categories like "Stuff."

C. Comparison Between FSF and SCF

To gain insights into the differences between the Feature Similarity Focus (FSF) and Spatial Continuity Focus (SCF) methods, we conduct a comparative analysis using Table V.

For the FSF method, with a CNN-Based backbone, the mIoU for "All" is 30.52, and for "Stuff," it is 42.39. On the other hand, the ResNet-18 backbone yields an mIoU of 30.07

for "All" and an impressive 54.10 for "Stuff." This indicates that FSF, particularly with a ResNet-18 backbone, excels in capturing semantic information related to complex and varied categories, such as "Stuff."

Moving to the SCF method, the mIoU for "All" with a CNN-Based backbone is 27.57, and for "Stuff," it is 35.08. Transitioning to a ResNet-18 backbone results in an improved mIoU of 30.52 for "All" and 42.37 for "Stuff." This suggests that SCF, like FSF, benefits from a more sophisticated backbone, and the ResNet-18 architecture contributes to better segmentation performance, especially for challenging categories like "Stuff."

To further refine the comparative analysis between the Feature Similarity Focus (FSF) and Spatial Continuity Focus (SCF) methods, we consider additional mIOU scores on BSD500 and PASCAL VOC2012 datasets, as presented in Table I.

In the BSD500 dataset, across different segmentation scenarios (All, Fine, and Coarse), FSF consistently outperforms SCF in terms of mIOU scores. Notably, for BSD500 All, FSF achieves an mIOU of 0.349 compared to SCF's 0.330. This pattern is observed in other scenarios, reinforcing the effectiveness of FSF in capturing fine-grained details and semantic nuances.

On the PASCAL VOC2012 dataset, both FSF and SCF demonstrate competitive performance, with FSF achieving an mIOU of 0.391 and SCF's 0.396. The marginal difference in mIOU scores on PASCAL VOC2012 suggests that both methods perform comparably on this specific dataset, indicating their capability to handle diverse segmentation challenges effectively.

Comparing the two methods across different datasets and segmentation scenarios, FSF consistently delivers higher mIOU scores, indicating its robustness and effectiveness in capturing both global and fine-grained semantic information. The choice of FSF over SCF is particularly beneficial when targeting scenarios with varied and intricate segmentation requirements.

Comparing the two methods, it is evident that both FSF and SCF show sensitivity to the choice of the backbone architecture, with ResNet-18 consistently outperforming CNN-Based backbones. FSF, however, exhibits higher mIoU values for "Stuff" across both backbones, emphasizing its effectiveness in capturing detailed and intricate features.

In conclusion, the choice between FSF and SCF should consider the specific requirements of the segmentation task, with FSF showing promise for scenarios involving complex and diverse categories, particularly when coupled with a ResNet-18 backbone.

VI. CONCLUSION

In conclusion, our study introduces a state-of-the-art unsupervised image segmentation approach that effectively overcomes the limitations of supervised methods, which heavily depend on costly pixel-level annotations. The dynamic weighting scheme, Silhouette Score Phase, integration of a pre-trained ResNet feature extraction, and Feature Pyramid

Network (FPN) decoding collectively contribute to superior performance. Remarkably, our method achieves the pinnacle of segmentation accuracy without extensive parameter tuning, showcasing adaptability across diverse datasets. Our approach establishes itself as a state-of-the-art solution through extensive quantitative evaluation, demonstrating its efficacy in real-world applications.



Boujemaa Guermazi is a researcher and academician in Electrical and Computer Engineering at Toronto Metropolitan University. His research interests encompass deep learning, image segmentation, and unsupervised machine learning. He earned his M.Sc Degree in Signals, Systems, and Data from the National Engineering School of Tunis in 2018. Before that, he completed a M.Sc Degree in Aircraft Operation Engineering - Pilot Engineer at the Aviation School of Borj El Amri in 2010. Boujemaa is dedicated to advancing the understanding and

application of cutting-edge technologies in the engineering sciences.



Riadh Ksantini received the M.Sc. and Ph.D. degrees in Computer Science from the Université de Sherbrooke, Sherbrooke, QC, Canada, in 2003 and 2007, respectively. Presently, he is Associate Professor at the Department of Computer Science, College of IT, University of Bahrain, Adjunct Associate Professor at the School of Computer Science, within the Faculty of Science of the University of Windsor, and Adjunct Professor at the Department of Computer Science, Université du Québec à Montréal (UQAM). His research interests include Artificial Intelligence,

Machine/Deep Learning, Pattern Recognition and Computer Vision.



Naimul Khan (Senior member, IEEE) is an associate professor in the electrical, computer, and biomedical engineering department at Toronto Metropolitan University. His research interest is in the user-centric intelligent systems combining machine learning and image processing. He has over 80 publications in this areas, backed by significant funding from government agencies and several awards.

REFERENCES

- [1] K. Ramesh, G. K. Kumar, K. Swapna, D. Datta, and S. S. Rajest, "A review of medical image segmentation algorithms," *EAI Endorsed Transactions on Pervasive Health and Technology*, vol. 7, no. 27, pp. e6–e6, 2021.
- [2] L. Zhao, H. Zhou, X. Zhu, X. Song, H. Li, and W. Tao, "Lif-seg: Lidar and camera image fusion for 3d lidar semantic segmentation," *IEEE Transactions on Multimedia*, 2023.
- [3] I. Ruban, V. Khudov, O. Makoveichuk, H. Khudov, and I. Khizhnyak, "A swarm method for segmentation of images obtained from on-board optoelectronic surveillance systems," in *2018 International Scientific-Practical Conference Problems of Infocommunications. Science and Technology (PIC S&T)*. IEEE, 2018, pp. 613–618.
- [4] Ç. Kaymak and A. Uçar, "A brief survey and an application of semantic image segmentation for autonomous driving," *Handbook of Deep Learning Applications*, pp. 161–200, 2019.
- [5] G. Gao, G. Xu, J. Li, Y. Yu, H. Lu, and J. Yang, "Fbsnet: A fast bilateral symmetrical network for real-time semantic segmentation," *IEEE Transactions on Multimedia*, 2022.
- [6] A. M. Hafiz and G. M. Bhat, "A survey on instance segmentation: state of the art," *International journal of multimedia information retrieval*, vol. 9, no. 3, pp. 171–189, 2020.
- [7] A. Kirillov, K. He, R. Girshick, C. Rother, and P. Dollár, "Panoptic segmentation," in *Proceedings of the IEEE/CVF conference on computer vision and pattern recognition*, 2019, pp. 9404–9413.
- [8] M. Kass, A. Witkin, and D. Terzopoulos, "Snakes: Active contour models," *International Journal of Computer Vision*, vol. 1, no. 4, pp. 321–331, jan 1988.
- [9] J. et all, "Some methods for classification and analysis of multivariate observations," *Proceedings of the fifth Berkeley symposium on mathematical statistics and probability*, vol. 1, no. 14, pp. 281–297, 1967.
- [10] P. F. Felzenszwalb and D. P. Huttenlocher, "Efficient Graph-Based Image Segmentation," *International Journal of Computer Vision*, vol. 59, no. 2, pp. 167–181, sep 2004.
- [11] Z. Liu, R. Shi, L. Shen, Y. Xue, K. N. Ngan, and Z. Zhang, "Unsupervised salient object segmentation based on kernel density estimation and two-phase graph cut," *IEEE Transactions on Multimedia*, vol. 14, no. 4, pp. 1275–1289, 2012.
- [12] P. Doll, R. Girshick, and F. Ai, "Mask R-CNN," *CVPR*, 2017.
- [13] W. Kim, A. Kanazaki, and M. Tanaka, "Unsupervised Learning of Image Segmentation Based on Differentiable Feature Clustering," *IEEE Transactions on Image Processing*, vol. 29, pp. 8055–8068, 2020.
- [14] B. Guermazi, R. Ksantini, and N. Khan, "A dynamically weighted loss function for unsupervised image segmentation," in *2022 IEEE Eighth International Conference on Multimedia Big Data (BigMM)*. IEEE, 2022, pp. 73–78.
- [15] G. Algan and I. Ulusoy, "Image classification with deep learning in the presence of noisy labels: A survey," *Knowledge-Based Systems*, vol. 215, p. 106771, 2021.
- [16] S. S. A. Zaidi, M. S. Ansari, A. Aslam, N. Kanwal, M. Asghar, and B. Lee, "A survey of modern deep learning based object detection models," *Digital Signal Processing*, vol. 126, p. 103514, 2022.
- [17] M. Cheriet, J. N. Said, and C. Y. Suen, "A recursive thresholding technique for image segmentation," *IEEE transactions on image processing*, vol. 7, no. 6, pp. 918–921, 1998.
- [18] T. Leung and J. Malik, "Contour continuity in region based image segmentation," *Computer Vision—ECCV'98: 5th European Conference on Computer Vision Freiburg, Germany, June, 2–6, 1998 Proceedings, Volume 1 5*, pp. 544–559, 1998.
- [19] S. S. Al-amri, N. V. Kalyankar, and K. S.D, "Image segmentation by using edge detection," *International Journal on Computer Science and Engineering*, vol. 2, no. 3, pp. 804–807, 2010.
- [20] N. Navab, J. Hornegger, W. M. Wells, and A. Frangi, *Medical Image Computing and Computer-Assisted Intervention—MICCAI 2015: 18th International Conference, Munich, Germany, October 5–9, 2015, Proceedings, Part III*. Springer, 2015, vol. 9351.
- [21] V. Badrinarayanan, A. Kendall, and R. Cipolla, "Segnet: A deep convolutional encoder-decoder architecture for image segmentation," *IEEE transactions on pattern analysis and machine intelligence*, vol. 39, no. 12, pp. 2481–2495, 2017.
- [22] L.-C. Chen, G. Papandreou, I. Kokkinos, K. Murphy, and A. L. Yuille, "DeepLab: Semantic image segmentation with deep convolutional nets, atrous convolution, and fully connected crfs," *IEEE transactions on pattern analysis and machine intelligence*, vol. 40, no. 4, pp. 834–848, 2017.
- [23] J. Zhuang, J. Yang, L. Gu, and N. Dvornek, "Shelfnet for fast semantic segmentation," in *Proceedings of the IEEE/CVF international conference on computer vision workshops*, 2019, pp. 0–0.
- [24] K. Simonyan and A. Zisserman, "Very deep convolutional networks for large-scale image recognition," *arXiv preprint arXiv:1409.1556*, 2014.
- [25] A. Hatamizadeh, Y. Tang, V. Nath, D. Yang, A. Myronenko, B. Landman, H. R. Roth, and D. Xu, "Unetr: Transformers for 3d medical image segmentation," in *Proceedings of the IEEE/CVF winter conference on applications of computer vision*, 2022, pp. 574–584.
- [26] M. Tran, L. Ly, B.-S. Hua, and N. Le, "Ss-3dcapsnet: Self-supervised 3d capsule networks for medical segmentation on less labeled data," in *2022 IEEE 19th International Symposium on Biomedical Imaging (ISBI)*. IEEE, 2022, pp. 1–5.
- [27] B. Zhou, H. Zhao, X. Puig, S. Fidler, A. Barriuso, and A. Torralba, "Scene parsing through ade20k dataset," in *Proceedings of the IEEE conference on computer vision and pattern recognition*, 2017, pp. 633–641.
- [28] Y. LeCun, C. Cortes, C. Burges *et al.*, "Mnist handwritten digit database," 2010.
- [29] A. Krizhevsky, "Learning multiple layers of features from tiny images," University of Toronto, Tech. Rep., 2009.
- [30] X. Ji, J. F. Henriques, and A. Vedaldi, "Invariant information clustering for unsupervised image classification and segmentation," *Proceedings of the IEEE/CVF international conference on computer vision*, pp. 9865–9874, 2019.
- [31] A. L. Rezaabad and S. Vishwanath, "Learning representations by maximizing mutual information in variational autoencoders," in *2020 IEEE International Symposium on Information Theory (ISIT)*. IEEE, 2020, pp. 2729–2734.
- [32] Y. Ouali, C. Hudelot, and M. Tami, "Autoregressive Unsupervised Image Segmentation," *Lecture Notes in Computer Science (including subseries Lecture Notes in Artificial Intelligence and Lecture Notes in Bioinformatics)*, vol. 12352 LNCS, pp. 142–158, 2020.
- [33] C. Han, L. Rundo, R. Araki, Y. Nagano, Y. Furukawa, G. Mauri, H. Nakayama, and H. Hayashi, "Combining noise-to-image and image-to-image GANs: Brain MR image augmentation for tumor detection," *IEEE Access*, vol. 7, pp. 156966–156977, 2019.
- [34] J. J. Hwang, S. Yu, J. Shi, M. Collins, T. J. Yang, X. Zhang, and L. C. Chen, "SegSort: Segmentation by discriminative sorting of segments," *Proceedings of the IEEE International Conference on Computer Vision*, vol. 2019-October, pp. 7333–7343, 2019.
- [35] L. Melas-Kyriazi, C. Rupprecht, I. Laina, and A. Vedaldi, "Finding an unsupervised image segmenter in each of your deep generative models," *arXiv preprint arXiv:2105.08127*, 2021.
- [36] J. Donahue and K. Simonyan, "Large scale adversarial representation learning," *Advances in Neural Information Processing Systems*, vol. 32, no. NeurIPS, pp. 1–11, 2019.
- [37] R. Abdal, P. Zhu, N. J. Mitra, and P. Wonka, "Labels4Free: Unsupervised Segmentation using StyleGAN," *Proceedings of the IEEE International Conference on Computer Vision*, pp. 13950–13959, 2021.
- [38] T. Karras, S. Laine, M. Aittala, J. Hellsten, J. Lehtinen, and T. Aila, "StyleGANv2," *Proceedings of the IEEE Computer Society Conference on Computer Vision and Pattern Recognition*, pp. 8107–8116, 2020.
- [39] X. Xia and B. Kulis, "W-Net: A Deep Model for Fully Unsupervised Image Segmentation," *arXiv*, nov 2017. [Online]. Available: <http://arxiv.org/abs/1711.08506>
- [40] L. Zhou and W. Wei, "DIC: Deep Image Clustering for Unsupervised Image Segmentation," *IEEE Access*, vol. 8, pp. 34481–34491, 2020.
- [41] S. E. Mirsadeghi, A. Royat, and H. Rezafooghi, "Unsupervised Image Segmentation by Mutual Information Maximization and Adversarial Regularization," *IEEE Robotics and Automation Letters*, vol. 6, no. 4, pp. 6931–6938, 2021.
- [42] J. H. Cho, U. Mall, K. Bala, and B. Hariharan, "Picie: Unsupervised semantic segmentation using invariance and equivariance in clustering," in *Proceedings of the IEEE/CVF Conference on Computer Vision and Pattern Recognition*, 2021, pp. 16794–16804.
- [43] W. Zhang, J. Pang, K. Chen, and C. C. Loy, "Dense siamese network for dense unsupervised learning," in *European Conference on Computer Vision*. Springer, 2022, pp. 464–480.
- [44] A. Kanazaki, "Unsupervised Image Segmentation by Backpropagation," *Icassp*, pp. 2–4, 2018.
- [45] K. He, X. Zhang, S. Ren, and J. Sun, "Deep residual learning for image recognition," in *Proceedings of the IEEE conference on computer vision and pattern recognition*, 2016, pp. 770–778.
- [46] H. Caesar, J. Uijlings, and V. Ferrari, "Coco-stuff: Thing and stuff classes in context," in *Proceedings of the IEEE conference on computer vision and pattern recognition*, 2018, pp. 1209–1218.

- [47] D. Martin, C. Fowlkes, D. Tal, and J. Malik, "A database of human segmented natural images and its application to evaluating segmentation algorithms and measuring ecological statistics," in *Proc. 8th Int'l Conf. Computer Vision*, vol. 2, July 2001, pp. 416–423.
- [48] M. Everingham, M. Everingham, A. Zisserman, A. Zisserman, C. Williams, and C. Williams, "The PASCAL Visual Object Classes Challenge 2006 (VOC2006) results," *International Journal of Computer Vision*, vol. 88, no. 2, pp. 303–338, 2010.
- [49] D. Batra, A. Kowdle, D. Parikh, J. Luo, and T. Chen, "icoseg: Interactive co-segmentation with intelligent scribble guidance," in *2010 IEEE computer society conference on computer vision and pattern recognition*. IEEE, 2010, pp. 3169–3176.
- [50] A. Kanazaki, "Unsupervised image segmentation by backpropagation," in *2018 IEEE international conference on acoustics, speech and signal processing (ICASSP)*. IEEE, 2018, pp. 1543–1547.
- [51] B. Guermazi, "Dynaseg-scf," Online video, 2024, accessed: March 15, 2024. [Online]. Available: https://drive.google.com/file/d/1q1tjtMB9Gf-3opqYb-kaM1_7MogQfctN/view?usp=sharing